Local-heterogeneous responses and transient dynamics of cage breaking and formation in colloidal fluids

Preetom Nag, Hiroshi Teramoto, Chun-Biu Li, Joseph Z. Terdik, Norbert F. Scherer, and Tamiki Komatsuzaki

Citation: The Journal of Chemical Physics **141**, 104907 (2014); doi: 10.1063/1.4894866
View online: http://dx.doi.org/10.1063/1.4894866
View Table of Contents: http://scitation.aip.org/content/aip/journal/jcp/141/10?ver=pdfcov
Published by the AIP Publishing

Local-heterogeneous responses and transient dynamics of cage breaking and formation in colloidal fluids

Preetom Nag,[1,2] Hiroshi Teramoto,[1,2] Chun-Biu Li,[2] Joseph Z. Terdik,[3,4,a)]
Norbert F. Scherer,[4,b)] and Tamiki Komatsuzaki[1,2,c)]
[1]*Graduate School of Life Science, Transdisciplinary Life Science Course, Hokkaido University, Kita 12, Nishi 6, Kita-ku, Sapporo 060-0812, Japan*
[2]*Molecule and Life Nonlinear Sciences Laboratory, Research Institute for Electronic Science, Hokkaido University, Kita 20 Nishi 10, Kita-ku, Sapporo 001-0020, Japan*
[3]*Department of Physics, University of Chicago, 5720 S. Ellis Ave, Chicago, Illinois 60637, USA*
[4]*Department of Chemistry, University of Chicago, 929 E. 57th St., Chicago, Illinois 60637, USA*

(Received 12 June 2014; accepted 25 August 2014; published online 11 September 2014)

Quantifying the interactions in dense colloidal fluids requires a properly designed order parameter. We present a modified bond-orientational order parameter, $\bar{\psi}_6$, to avoid problems of the original definition of bond-orientational order parameter. The original bond-orientational order parameter can change discontinuously in time but our modified order parameter is free from the discontinuity and, thus, it is a suitable measure to quantify the dynamics of the bond-orientational ordering of the local surroundings. Here we analyze $\bar{\psi}_6$ in a dense driven monodisperse quasi-two-dimensional colloidal fluids where a single particle is optically trapped at the center. The perturbation by the trapped and driven particle alters the structure and dynamics of the neighboring particles. This perturbation disturbs the flow and causes spatial and temporal distortion of the bond-orientational configuration surrounding each particle. We investigate spatio-temporal behavior of $\bar{\psi}_6$ by a Wavelet transform that provides a time-frequency representation of the time series of $\bar{\psi}_6$. It is found that particles that have high power in frequencies corresponding to the inverse of the timescale of perturbation undergo distortions of their packing configurations that result in cage breaking and formation dynamics. To gain insight into the dynamic structure of cage breaking and formation of bond-orientational ordering, we compare the cage breaking and formation dynamics with the underlying dynamical structure identified by Lagrangian Coherent Structures (LCSs) estimated from the finite-time Lyapunov exponent (FTLE) field. The LCSs are moving separatrices that effectively divide the flow into distinct regions with different dynamical behavior. It is shown that the spatial distribution of the FTLE field and the power of particles in the wavelet transform have positive correlation, implying that LCSs provide a dynamic structure that dominates the dynamics of cage breaking and formation of the colloidal fluids.
 [http://dx.doi.org/10.1063/1.4894866]

I. INTRODUCTION

Dynamical heterogeneity (DH) is one of the most intriguing subjects in soft matter and biological physics, as it is a defining property of amorphous materials, dense colloidal fluids,[1,2] sheared granular media,[3,4] and super-cooled liquids.[5,6] DH exists in all disordered materials with glassy transitions that occur intermittently with waiting or relaxation times that are broadly distributed. DH is usually composed of a succession of confinement events of a particle by neighboring particles. This cage effect and the breakages of the cages and transitions to diffuse, account for the variability of different relaxation timescales.[7,8] For short times, a particle is confined by its neighboring particles in a cage whose timescale of confinement varies from place to place. On long timescales the particle manages to break its cage, so that it is able to diffuse through the entire system by successive cage breaking.

The main feature of DH involves spatial and dynamical correlations among particles that undergo large ("mobile") displacements over a suitably chosen time interval. Spatially correlated mobile particles move cooperatively in a fashion that they follow one another[9] and form quasi-one-dimensional, stringlike clusters.[10] Particles that are dynamically correlated can be investigated by constructing a four-point susceptibility where the dynamical correlation length grows by increasing the density of the fluid.[11] Studies of DH also include topological persistence as measured by two overlapping order parameters that quantify the correlation between particle configurations at different times.[12]

Understanding DH in granular systems subjected to a mechanical perturbation is of considerable interest.[13–17] Several experiments on granular systems have emphasized the role of DH under shear perturbation[3,18] and particle dragging.[19–21] Recent experimental techniques that involve optical or magnetic tweezers coupled with optical microscopy in colloidal systems[22,23] allow a trapped particle to provide a precise

a)Current address: Department of Physics, Harvard University, Cambridge, Massachusetts 02138, USA.
b)Electronic mail: nfschere@uchicago.edu
c)Electronic mail: tamiki@es.hokudai.ac.jp. URL: http://mlns.es.hokudai.ac.jp/.

and localized mechanical perturbation to the system and to detect the response of the system simultaneously. This enables investigating the microscopic origin of complex fluid behavior, such as microviscosities in the shear thickening and shear thinning regimes as a function of the speed of the probe particle.[24,25] By applying a force to the probe particle, one can explore the instantaneous and average structural responses[26] and the spatial reorganization during and after the perturbation.[27] However, the interplay between DH and the spatio-temporal behavior of the caging of particles by their neighbors is still poorly understood.

The so-called bond-orientational order parameter,[28–30] ψ_6, has often been used in quasi-two-dimensional (q2D) colloidal fluids,[26,31–33] in order to quantify how nearby particles are closely packed to a reference particle, i.e., in the form of a hexagonal configuration. Dynamics of ψ_6 was studied in granular liquids near the glass transition to probe the dynamical heterogeneity and slow dynamics. There, the spatial distribution of the time-average of ψ_6 was investigated in order to extract slow dynamics of the medium-range crystalline ordered particles, whose long-range ordering is prevented by frustration effects.[33] This time-average was taken over the structural relaxation time. However, relaxation process may proceed over several timescales and some structural cage breaking and formation may occur in shorter times than a timescale used for the time-averaging. If so, it is difficult to determine properly when and how the structural breakage and formation events happen and which particles are involved in those structural events in terms of the time-averaged spatial distribution of the bond-orientational order parameter.

In this paper, we focus on the time dependence and spatial extent of bond-orientational ordering around individual particles in order to see how colloidal particles are involved in the cage breaking and formation dynamics in response to a microscopic perturbation imposed by a particle which is trapped at the center and the fluid moving around it.[26] We first introduce a modified bond-orientational order parameter, denoted by $\bar{\psi}_6$, to properly quantify the time evolution of bond-orientational ordering. This overcomes some drawbacks that exist in the original definition of ψ_6. From the time evolution of $\bar{\psi}_6$ we observe that the size of temporal fluctuation in the magnitude of $\bar{\psi}_6$, not the magnitude of $\bar{\psi}_6$ itself, reflect the extent of distortion in the surrounding particles, i.e., cage breaking and formation. To see when and which particles participate in the cage breaking and formation dynamics, we perform a time-frequency analysis by continuous Wavelet transforms for the time series of $\bar{\psi}_6$. It is found that particles having frequency components similar to that of the inverse of the timescale of perturbation are involved in cage breaking and formation.

To look further into the origin of cage breaking and formation, we introduce the concept of Lagrangian Coherent Structures (LCSs) developed in dynamical systems theory,[34–36] which effectively divide the flow into distinct regions with qualitatively different past or future. In this paper, LCSs refer to the location of large magnitude in the finite-time Lyapunov exponent (FTLE) field where FTLE measures the maximum separation rate between nearby trajectories over a finite time interval. Due to the FTLE ridges, their spatio-temporal location is expected to affect the nearby packing configuration of the colloidal particles within the corresponding separation timescale. It is found that the spatio-temporal distribution of the FTLE field and the power of the particles in the wavelet transform, both computed for the same timescale, have a positive correlation, showing that FTLE based LCSs, denoted by FTLE/LCSs,[37] provide a dynamic structure that dominates the dynamics of cage breaking and formation of the colloidal fluids.

Our paper is organized as follows: In Sec. II we briefly describe the experimental system we study, overview and discuss some drawbacks of the original bond-orientational order parameter, provide a modified bond-orientational order parameter, and introduce the concept of FTLE/LCSs. Section III contains the investigation of the time series of the $\bar{\psi}_6$, the wavelet analysis to investigate the cage breaking dynamics, the results of FTLE/LCSs that probe the dynamical heterogeneity and the relationship between FTLE/LCSs and cage breaking dynamics. We provide conclusions and outlook in Sec. IV.

II. SYSTEM AND METHOD

A. A q2D system with a mechanical perturbation

The q2D experimental system considered in this paper was described in detail in Ref. 26. The sample consists of an aqueous suspension of uniform size silica spheres (diameter $d = 2.56 \pm 0.04$ μm) and the suspension is confined between two hard walls with height (separation) of 3.2 μm, i.e., slightly larger than the particle diameter. A particle is optically trapped at the center by a 810 nm laser beam with a force constant $k = 0.2$ pN/nm. The stage containing the suspension is moved at a constant speed v and thus the trapped particle interacts with and causes a mechanical perturbation to the system. The case considered has an average packing fraction of ~0.76. Note that the experimental data are collected in the reference frame of the trapped particle and the stage moves with a constant speed. One can easily transform the data into the dragged reference frame where the probe particle is dragged at constant speed and the stage is stationary. We do our analysis in the trapped reference frame. Note however that the quantities we analyze are frame-independent, i.e., do not depend on the reference frame in which one observes the system dynamics.

B. Bond-orientational order parameter and its drawback

How can one quantify spatio-temporal heterogeneity of local environments in the neighborhood of individual particles in colloidal fluids under a mechanical perturbation? In a quasi-two-dimensional (q2D) colloidal fluid, the packing structure around a particle of interest can be quantified by the so-called bond-orientational order parameter ψ_6^j defined as[26,31–33,38]

$$\psi_6^j = \frac{1}{n_j}\left|\sum_{k=1}^{n_j}\exp(i\cdot 6\theta_k^j)\right| \quad (1)$$

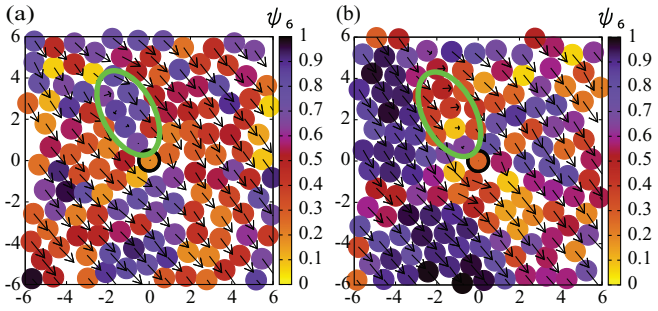

FIG. 1. (a) and (b) are two snapshots of ψ_6 of colloidal particles with their displacement vector under the steady flow from the left top to the right bottom, where the center particle trapped by the optical tweezer as outlined by black bold circle.

for each particle j, where the sum runs over n_j nearest neighbors around particle j, and θ_k^j is the angle between an arbitrary fixed axis and the link of particle j and its kth nearest neighbor. In Eq. (1), the summand term refers to the configuration of the first neighboring cage, and n_j is the corresponding number of the first neighboring particles around particle j. Usually, n_j is chosen either as a constant of value six, i.e., six nearest neighbors,[26,32] or as a variable dependent on local coordination around particle j (first nearest neighbors) defined by using a Voronoi construction.[31,33,38] The value $\psi_6^j = 1$ implies perfect hexatic order solely with six nearest neighboring particles, whereas $\psi_6^j \ll 1$ implies a region deviating from hexatic order.

Differences in the values of ψ_6 have been used to assign frozen (ordered) and mobile (disordered) regions, termed grain and grain boundary (GB) regions.[32] Particles in the GB regions are mobile, readily breaking their neighboring cages. They can be visualized by a snapshot of bond-orientational structure overlaying the mobile particles at the high packing fraction of 0.85.[32] However, at (comparatively) lower packing fraction, e.g., ∼0.76 in our q2D colloidal fluid system experiencing the constant dragging perturbation,[26] ordered and disordered regions are sparsely distributed and they are not directly related to the mobility of the particles. For example, particles in remote regions having lower values of ψ_6 simply passing along the flow applied to the colloidal system while maintaining the low ψ_6 values. To demonstrate it, Fig. 1 shows two representative snapshots of the distribution of ψ_6 of colloidal particles. In Fig. 1(a) some particles in front of the center particle along the steady flow (indicated by the green ellipse) get stuck and are slowed down for some time duration and have a large ψ_6 value (i.e., are ordered). However, in Fig. 1(b) at some later time, the ordered region disappears and becomes disordered with smaller ψ_6. In fact, regions of large and small ψ_6 vary in time and sometimes exchange with each other. Thus the instantaneous distribution of ψ_6 does not necessarily capture the imminent heterogeneous nature of the frozen and mobile regions. In this regard, the time variation of ψ_6 is more insightful to understand how the perturbation induces the rearrangement of particles' positions.

In quantifying the time evolution of packing structure around individual particles in colloidal fluids, some disadvantages emerge for the bond-orientational order parameter es-

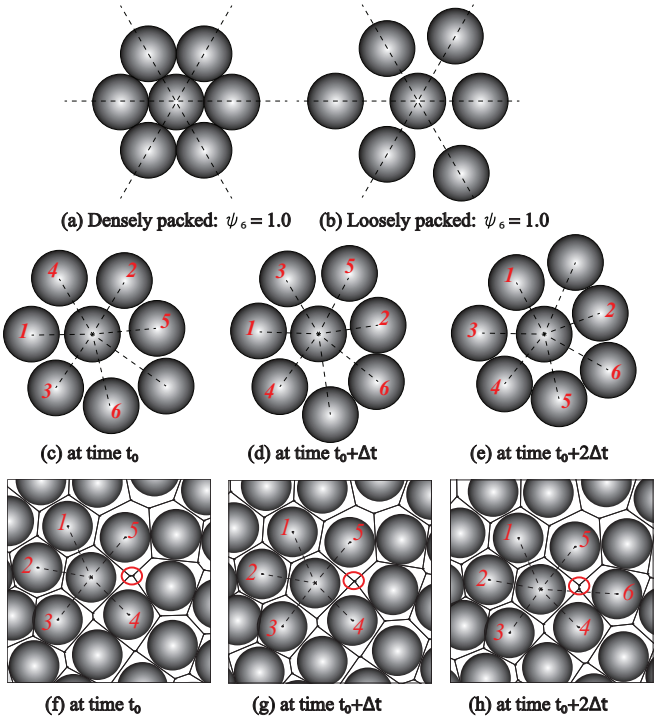

FIG. 2. (a) Densely packing and (b) loosely packing structures. Both return the same value of $\psi_6 (= 1)$. (c)–(e) One particle is surrounded by seven particles but which particles are the six nearest neighbors are different from time to time because of the fluctuation of their distance from the center particle. (f)–(h) Voronoi construction at successive time instants. Fluctuations in the particle positions result in different constructions in (g) to (h) because one triangular network in (f) becomes unstable in (g) and developed another network at that location in (h) as indicated by the red circle.

pecially at low packing fractions, e.g., 0.72–0.79. In Eq. (1), the summand term takes into account only the orientation (or angular position) of the neighboring particles. Therefore, ψ_6 gives the same value for the different cases shown in Figs. 2(a) and 2(b) since the angular positions of the surrounding particles are the same. Another problem is in the identification of the number of neighboring particles around particle j, n_j. One common choice is $n_j = 6$, that is, six nearest neighbors surrounding any particle of interest.[26,32] However, when a particle is surrounded by more than six particles in the first neighboring shell as described schematically in Figs. 2(c)–2(e) (it was found that about 12% of all particles have more than six particles there in our system), the identification of six *nearest* neighbors may change from time to time due to the fluctuation in positions. Therefore, ψ_6 may change discontinuously in time for particles that have more than six neighboring particles in the first shell for a certain time duration even when the actual configurational change of neighboring particles is smooth.

Another choice for n_j is to determine the neighboring particles from the shared edges of Voronoi tessellation.[33,38] As seen from Figs. 2(f)–2(h), the number of edges in a Voronoi cell and so the number of neighboring particles corresponding to the same particle, changes from Figs. 2(f)–2(h). That is, as indicated by the red circle, if one of the edges becomes very short compared to the others, the corresponding triangular network becomes unstable due to a fluctuation of the

particles' position. After some time another triangular network may develop at that location. As a result, the number of neighboring particles can change discontinuously and this causes (unphysical) discontinuous jumps in the values of ψ_6. Therefore, some modification is needed to eliminate these drawbacks.

C. A modified bond-orientational order parameter $\bar{\psi}_6$

We present a modified bond-orientational order parameter $\bar{\psi}_6$ to properly quantify the dynamical evolution of local packing structure. This parameter is defined as

$$\bar{\psi}_6^j \equiv \frac{\left|\sum_k' w(|\mathbf{r_k} - \mathbf{r_j}|) \exp\left(i \cdot 6\theta_k^j\right)\right|}{c_0}, \qquad (2)$$

where the summation $\sum_k'$ runs over all particles except the jth particle, θ_k^j is the angle between an arbitrary fixed axis and the link of the particles k and j whose positions are denoted by $\mathbf{r_k}$ and $\mathbf{r_j}$, respectively, c_0 is the maximum possible value of the denominator in case that the whole system attains perfect order (i.e., making $\bar{\psi}_6^j$ normalized as $0 \le \bar{\psi}_6^j \le 1$). The weight function $w(r) = \exp(-\frac{(r-d)^2}{2\sigma^2})$, d is the diameter of each particle, this weight function $w(r)$ takes into account the distance between the surrounding particles and the particle of interest. In order to choose the value of σ, we estimate the size of the first neighboring shell in terms of the radial distribution. In our system the radial distribution function has the well-defined first minimum placed at approximately $1.5d$ as seen in Fig. 3. The first minimum provides the characteristic length scale of the first neighboring shell. In our system σ is chosen so that particles in the first neighboring shell lie within two standard deviations, $2\sigma = 1.5d - d = 0.5d$ from the mean d, and hexagonal configurations such as Figs. 2(a) and 2(b) can be distinguished (e.g., $\bar{\psi}_6$, returns 1.0 and 0.567 for the configurations in Figs. 2(a) and 2(b), respectively). Another advantage is that this formula does not require identifying the neighboring particles, and is therefore free from any discontinuous identification of neighboring particles. Note that $\bar{\psi}_6$, like the original ψ_6, is a frame-independent measure.

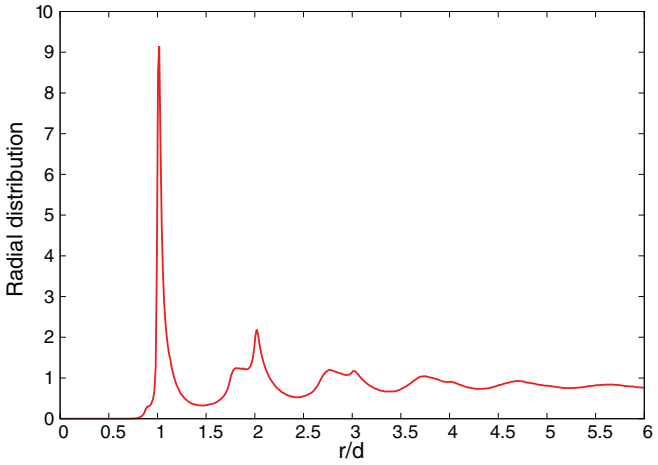

FIG. 3. Average radial distribution function of a colloidal fluid with an average packing fraction of 0.76. The Péclet number (Pe) for the dragging is 190. This radial distribution function is calculated by using configurations of the colloidal fluid observed for 74.61s with frame rate 67 Hz.

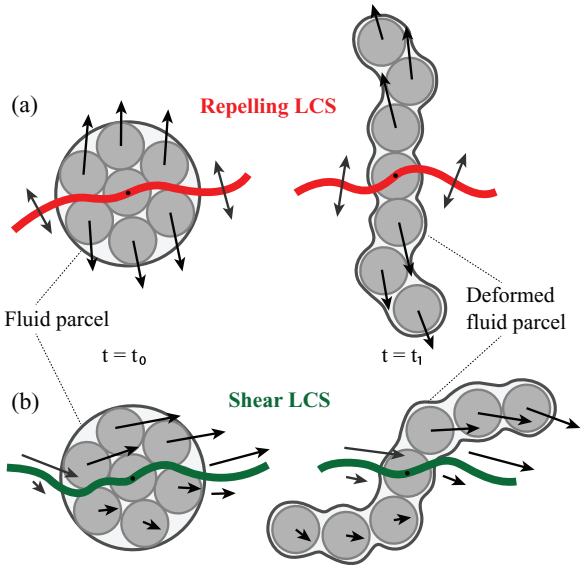

FIG. 4. Two types of deformation of a fluid parcel containing a set of particles over the time interval $[t_0, t_1]$. (a) For repelling LCS, this deformation occurs normal to it and (b) for shear type LCS, such deformation occurs tangential to it.

D. Lagrangian coherent structures

We introduce another concept, LCSs, to investigate underlying mechanism behind cage breaking and formation. The concept of Lagrangian Coherent Structures was first introduced by Haller[34,35] and has received significant attention for understanding transport phenomena in finite-time non-autonomous dynamical systems. Briefly, LCSs serve as robust transport barriers between regions in which particles have different dynamical behavior. By definition, LCSs are an invariant manifold across which any particle cannot traverse. Thus they are barriers to transport between the regions of different dynamics. Such structures can be characterized as co-dimension one (lines in two-, surfaces in three-dimensions) and play the dominant role in attracting, repelling or shearing of neighboring trajectories over a finite time interval $[t_0, t_1]$. Fig. 4 shows a schematic description of repelling and sheared type LCSs. Fig. 4(a) depicts a fluid parcel containing a set of particles initially at time $t = t_0$ is deformed along the normal direction to the repelling LCSs as it repels strongly the nearby fluid particles by time $t = t_1$. Fig. 4(b) depicts a fluid parcel that deforms along the tangential direction to the sheared LCS as the particles in the upper side move faster than those of the lower side.

The cornerstone of this structure is the frame-invariance property. To that end, when defining LCSs, the fluid motion is viewed from a Lagrangian, rather than an Euler perspective. A number of phenomena have been studied through LCSs including cell behavior,[39] blood flow mechanics inside blood vessels[36] and hearts,[40] prey-predator interaction in jelly fish feeding,[41] particle dynamics,[37] etc.

Based on the numerous application of LCSs, the most efficient and simplest diagnostic tool for identifying LCSs would be to identify the ridges or the location of high magnitude in the FTLE field.[42] Basically, at each location of the ridges, the FTLE possesses the maximum separation rate between nearby trajectories over a finite time interval. Maximum ridges of the FTLE field in forward-time propagation are indicators of repelling LCSs that are the regions of the locally strongest diverging flow in the system.[43,44] Performing the same procedure in backward-time propagation can identify maximum ridges of the backward-time FTLE field. The regions of the locally strongest diverging flow backward in time are, in fact, those of the locally strongest converging flow in ordinary forward-time propagation, corresponding to attracting LCSs in the system.

1. Mathematical background of LCSs

First let $\mathbf{x}(t, t_0, \mathbf{x_0}) \in \mathbb{R}^2$ be the position of a particle at time $t \in \mathbb{R}$, which starts from the initial position $\mathbf{x_0}$ at time t_0. Here we consider two dimensional space because the system in this paper can be regarded as a two-dimensional system as the motion of particles are confined between two hard walls and the height (distance) between two walls is only 1.5 times the diameter of particles.[26] We define a flow map, $\mathbf{F}^t_{t_0}(\mathbf{x_0}) = \mathbf{x}(t, t_0, \mathbf{x_0})$ that maps the initial position of a particle to its position after a time interval $T = t - t_0$. The largest FTLE $\Lambda^t_{t_0}(\mathbf{x_0})$ over the time interval $[t_0, t]$ is then defined as[34]

$$\Lambda^t_{t_0}(\mathbf{x_0}) = \frac{1}{|t - t_0|} \ln \sqrt{\lambda_{\max}\left(\mathbf{C}^t_{t_0}(\mathbf{x_0})\right)}, \tag{3}$$

where $\mathbf{C}^t_{t_0}(\mathbf{x_0}) = \left(\frac{d\mathbf{F}^t_{t_0}(\mathbf{x_0})}{d\mathbf{x_0}}\right)^* \frac{d\mathbf{F}^t_{t_0}(\mathbf{x_0})}{d\mathbf{x_0}}$ is the finite-time right Cauchy-Green deformation tensor, a rotation and translation invariant measure of deformation, where the symbol * refers to matrix transposition. $\lambda_{\max}(\mathbf{C}^t_{t_0}(\mathbf{x_0}))$ denotes the largest eigenvalue of $\mathbf{C}^t_{t_0}(\mathbf{x_0})$, which is always real and positive since $\mathbf{C}^t_{t_0}(\mathbf{x_0})$ is a symmetric and positive definite tensor by definition. Due to the frame-independence of the Cauchy-Green deformation tensor, the FTLE field is independent of choice of the reference frame. Basically, the largest eigenvalue and the corresponding eigenvector provides the maximal amount and the maximal principal stretching direction of the deformation of a fluid parcel. The distribution of the FTLE field in the phase space can be used to locate the maximum deformation of a fluid parcel in the dynamical system. Here, the locations of the high magnitude of FTLE values in the FTLE field are used to identify LCSs[45] and denoted by FTLE/LCSs.

2. Computation of FTLE/LCSs

The procedure described in Sec. II D 1 has been performed on an initial grid on which virtual particles are placed at time t_0 with a uniform spacing of $0.0125d$ in the domain of interest. The trajectories of the particles at time t, are obtained by constructing the flow map from instantaneous tracking[37] of colloid particle positions from the experimental data. The flow map is numerically differentiated with respect to the initial position of the particles to obtain the deformation tensor and subsequently the largest eigenvalue of the tensor. The FTLE value is then computed for each particle in the grid and assigned to the particle location at time t_0. This process is repeated for various initial times t_0 to get the time evolution of the FTLE field. In general, one can choose an integration time corresponding to the timescale of the dynamics of interest. However, it is not desirable to choose the integration time larger than the timescale in which all the particles are advected out from the spatial domain.

III. RESULTS AND DISCUSSION

A. Investigation of the time series of $\bar{\psi}_6$ for some particles

Fig. 5 shows a representative snapshot of $\bar{\psi}_6$ at one time instant, which shows that, at this packing fraction of ~0.76, there exist no clear grain and grain boundary regions. Turning to the time evolution of $\bar{\psi}_6(t)$, it has been found that $\bar{\psi}_6(t)$ of the center particle, which is optically trapped, exhibits the largest fluctuation along the time propagation. Some other particles also exhibit a similar large variation of $\bar{\psi}_6(t)$ when they are passing through the neighborhood of the center particle and/or in front of the center particle (see Video 1 in the supplementary material[46]). Fig. 6 exemplifies the time evolution of $\bar{\psi}_6(t)$ for some randomly selected particles. In the plot at the lower-middle image of the figure, each colored circle represents the position of a randomly selected colloidal particle at a certain time instant with a line passing through the circle corresponding to the trajectory of the corresponding particle. The number inside the circle is the particle's index. The trapped particle is located at the center. The time series of $\bar{\psi}_6(t)$ of the selected particles are superposed to that of $\bar{\psi}_6(t)$ of the probe particle, as indicated by the red line. From the

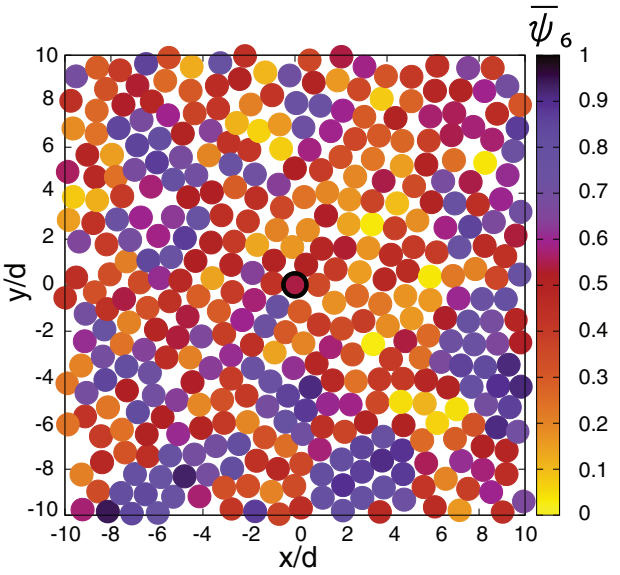

FIG. 5. A snapshot of $\bar{\psi}_6$ in the colloidal fluids at the packing fraction of ~0.76. The darker (the lighter or the more yellowish) the color, the closer (the looser) to hexagonal packing the nearby configuration is.

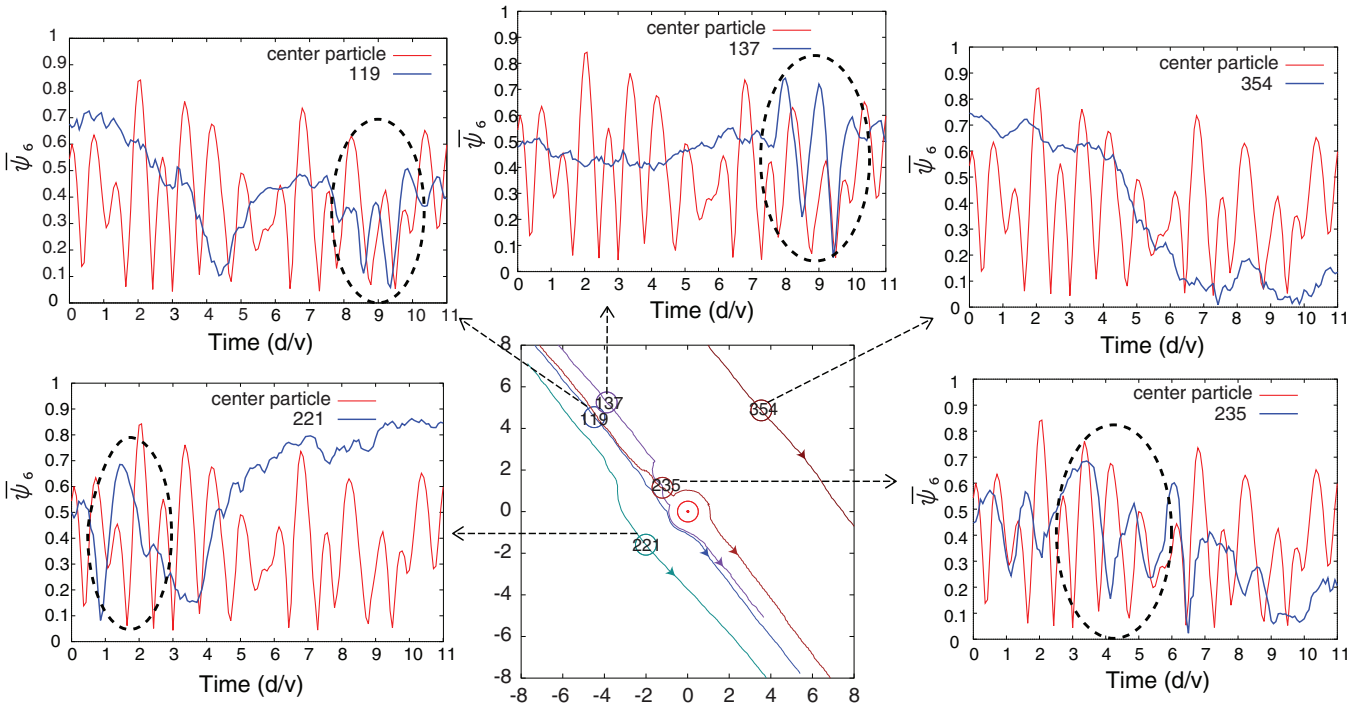

FIG. 6. Time series of $\bar{\psi}_6(t)$ of some randomly chosen particles, as shown in the lower-middle panel, is superposed to that of the probe particle for comparison. The unit of time on the horizontal axis is d/v where d and v denotes, respectively, the diameter of each particle and the constant speed applied to the system except the trapped probe particle. One can see that the time period of one oscillation in the fluctuation of $\bar{\psi}_6(t)$ of the probe particle is found to be an order of unity in the unit of d/v.

superposition of the time series, we can see that variations of $\bar{\psi}_6(t)$ for particles 119, 137, 221, 235, at some time duration, are roughly similar to those of the probe particle as indicated by dotted ellipses. In fact, at these time durations the corresponding particles are passing through the neighborhood of the probe particle. However, for particle 354, such a significant local and fast fluctuation of $\bar{\psi}_6(t)$ seems not to exist; it simply "passively" passes through the remote region from the center particle.

Fig. 7 illustrates the underlying configurational changes corresponding to the fluctuation of $\bar{\psi}_6$ for the center particle (indicated by the red circle) and two other particles of index 119 and 137 (blue circles). Here the particles surrounding the center particle, and also particles of index 119 and 137, are chosen within the radial distance of $1.5d$ from them (since particles in the first neighboring shell lie within $1.5d$ from a particular particle). The vectors (magnified by two times) on the particle represent their displacements in time $0.5d/v$. Fig. 7(a) shows that the packing structure for the probe particle is repeatedly breaking and more likely forming in a hexagonal shape which is quantified by $\bar{\psi}_6$. One can see that for the center particle, this fluctuation more likely occurs in the timescale ($\sim d/v$) as the center particle needs to move one particle's diameter (d) through breaking its first neighboring cage at the constant speed v. Within this timescale, the surrounding medium will also be perturbed and this perturbation causes a rearrangement of the packing structure around some other particles. For example, in Fig. 7, particles of index 119 and 137 show that, along the plateau regions of $\bar{\psi}_6(t)$, that is, from 6 to 7.5 d/v for particles 119 and 137, their packing configuration is not changing significantly. In this time regime, surrounding particles simply move parallel to the constant velocity vector $\boldsymbol{v}$ applied to the system and the displacement vectors of the surrounding particles are similar to each other. However, whenever the displacement vectors of the surrounding particles become not parallel, $\bar{\psi}_6(t)$ starts to fluctuate with large amplitude. Such large fluctuation starts from $\sim 8d/v$ for both the particles when some nearby particles seem to get stuck and slow down as illustrated by the displacement vectors. This shows that fluctuations in the magnitude of $\bar{\psi}_6(t)$ manifest the dynamical heterogeneity in the neighborhood of the corresponding particles. It should also be noted that the timescale of the fluctuations in $\bar{\psi}_6(t)$ for these particles look similar to that for the center particle.

B. Wavelet analysis for the time series of $\bar{\psi}_6$

In order to quantitatively investigate the spatio-temporal behavior of the time variation of $\bar{\psi}_6(t)$, we employ continuous wavelet transform to $\bar{\psi}_6(t)$ and focus on the frequency component corresponding to the timescale of the perturbation by the probe particle. A set of particles that contain the frequency component appearing in a certain time duration along the time propagation can be considered as ones that respond to the perturbation. Wavelet transform analysis involves a transformation from a time series $\bar{\psi}_6(t)$ with multiplication by a window function called a wavelet function. In brief, this wavelet function operates along the time series with dilation and compression of the support of the window function, and the wavelet transform quantifies the local matching of the wavelet with the time series. If the wavelet matches well with the time series at a specific scale and location, then a large transformed value

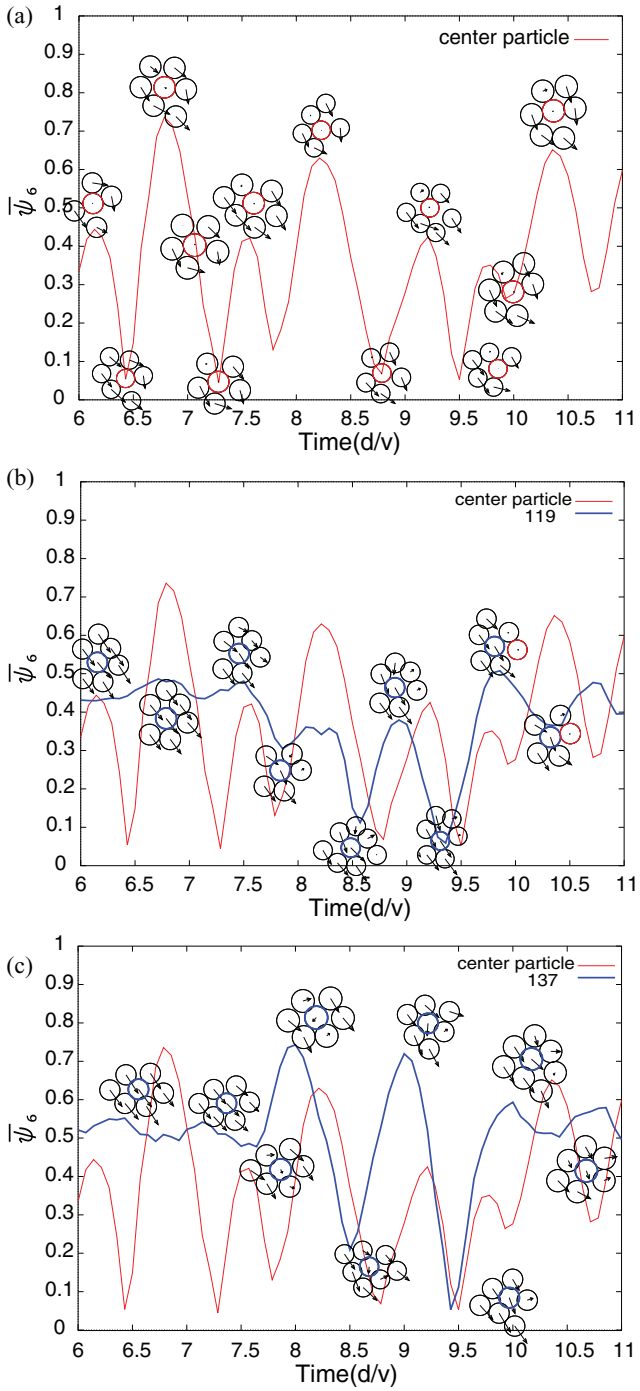

FIG. 7. A series of snapshots of local configurations in the neighborhood of a particle along the time evolution associated with $\bar{\psi}_6(t)$. (a) The center particle, (b) particle 119, and (c) particle 137. The vectors indicate the displacements of the corresponding particle in time $0.5d/v$ and the center particle and particles 119 and 137 are indicated by red and blue circles, respectively. In (b) and (c) $\bar{\psi}_6(t)$ of the center particle is also shown for comparison. In (b) particle 119 undergoes direct collision to the center particle near the time $10\,d/v$, but in (c) particle 137 does not.

is obtained. Otherwise a small value is obtained. The transform is computed at various locations of the signal and for various scales of the wavelet, thus filling a two dimensional timescale plane. The continuous version of this transform is called continuous wavelet transform (CWT). It is defined as[47]

$$CWT^{\phi}_{\bar{\psi}_6}(\tau, s) = \frac{1}{\sqrt{s}} \int \bar{\psi}_6(t)\phi\left(\frac{t-\tau}{s}\right) \mathrm{d}t, \tag{4}$$

which is a function of two variables, τ and s, the translation and scale parameters, respectively. $\phi(t)$ is called the wavelet function. Note that the scale parameter s has a reciprocal relationship with frequency f, i.e., $s = f_b/f$, where f_b is the base frequency of the wavelet function. Therefore, we can rewrite Eq. (4) as a function of τ and f as

$$\widetilde{CWT}^{\phi}_{\bar{\psi}_6}(\tau, f) = \sqrt{\frac{f}{f_b}} \int \bar{\psi}_6(t)\phi\Big(\frac{f(t-\tau)}{f_b}\Big) \mathrm{d}t. \tag{5}$$

For the wavelet function, in this paper, we choose the Gabor wavelet[48] defined as

$$\phi(t) = \frac{1}{\sqrt{w}}(e^{i2\pi\nu t/w} - e^{-\pi\nu^2})e^{-\pi(t/w)^2}, \tag{6}$$

with width parameter w and frequency parameter ν. This function is a Gaussian modulated by a sinusoid. The width parameter w controls the width of the region over which $\phi(t)$ is concentrated. The smaller the value of w, the more $\phi(t)$ is confined to a smaller interval of the time axis. The value ν/w is the base frequency for the Gabor wavelet, and hence the window size depends on the value of the base frequency to be monitored. Note that there is always uncertainty between the time and frequency resolution of the window function used in the wavelet analysis: the wider (narrower) the window size, w, the better (worse) the resolution in frequency but the worse (better) the resolution in time. Several ways have been proposed to find the uncertainty bound, and the most common one is the product of the standard deviations in the time and frequency domain. Among all kinds of window functions, the Gabor wavelet is known to achieve the lowest bound and obtain the best analytical resolution in the time and frequency domain.[48]

In the computation, we set $\nu = 1, w = d/v$ so that the timescale of the base frequency f_b corresponds to the timescale of the perturbation applied to the probe particle, i.e., $f_b = v/d = 0.07324$/frame where $v = 0.1875$ μm/frame is the flow velocity applied to the system and $d = 2.56$

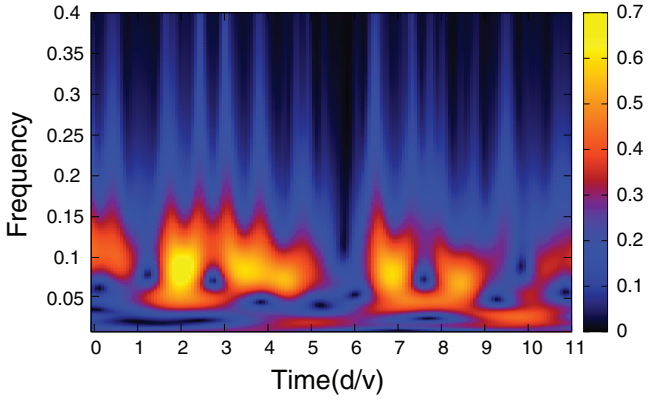

FIG. 8. The $\widetilde{CWT}$ scalogram for the time series of bond-orientational structure $\bar{\psi}_6$ of the probe particle. The color bar represents the magnitude of the Gabor wavelet transform in a two-dimensional time-frequency plane.

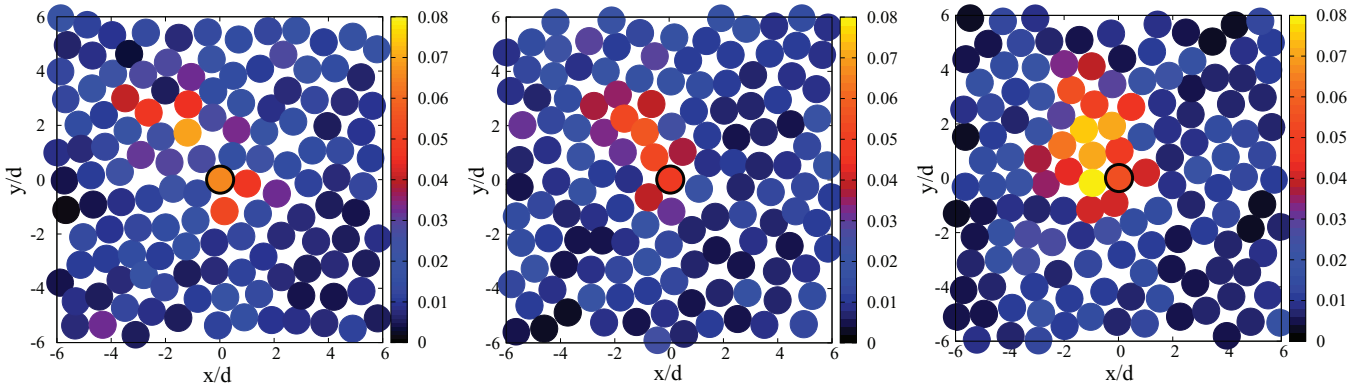

FIG. 9. $P(t)$ for colloidal particles is plotted at several values of time t. The color bar represents the total power in the wavelet transform. Brighter color corresponds to higher power, therefore, contains the frequency components of interest, involving cage breaking and formation dynamics. The (optically trapped) center particle is outlined by the black circle.

± 0.04 μm is the diameter of particles. In principle, w can be determined irrespective of any value of f_b, and, thus, as long as we increase the value of ν, the width parameter w also increases (in order to keep $f_b(=\nu/w)$ constant). This implies that we could obtain higher frequency resolution but at the same time we will lose the time resolution due to the filtering of larger w. Because of the reciprocal relationship between scale and frequency, the value of $\nu = 1$ provides modest resolution in both frequency and time in the wavelet transform.[49]

The magnitude-scalogram of the Gabor wavelet transform for the probe particle is shown in the two-dimensional time-frequency plane in Fig. 8 as evaluated from Eq. (5). Indeed, in our calculation, we varied frequencies from 0.0078 to 0.5, the Nyquist frequency. One can see that, with the above choice of ν and w, this scalogram has significant frequency components around f_b (corresponding to the yellowish bright regions). As a reminder, the bond-orientational ordering in Figs. 6 and 7(a) in the vicinity of the center particle appears and disappears repeatedly under the perturbation to the particle. From the corresponding trajectory of $\bar{\psi}_6(t)$ (Fig. 7(a)), the value of $\bar{\psi}_6(t)$ is relatively small <0.5 and one particle seems to get stuck in front of the probe particle at these time regimes. Likewise, the bright regions appear roughly in an "oscillatory" manner in Fig. 8 and there exist some time regimes where the frequency components around f_b are absent (e.g., at time 1, 5-6, 7.5, 9.5 d/v).

Particles whose $\widetilde{CWT}$ scalograms consist of such frequency components are expected to be involved in cage breaking and formation dynamics on some timescale when those components emerge. In order to evaluate the existence of such frequency components we calculate the power of the wavelet transform at each time t, as defined as

$$P(t) = \int_{f_b-\sigma_{f_b}}^{\text{Nyquist frequency}} A(f,t)\mathrm{d}f, \tag{7}$$

where $A(f, t)$ is defined as $A(f,t) = |\widetilde{CWT}^{\phi}_{\bar{\psi}_6}(t, f)|$ and $\sigma_{f_b} \approx 0.03$ is the amount of uncertainty for the frequency component f_b. This uncertainty arises because of the finite size of the window function and can be evaluated from the Fourier transform of the Gabor wavelet.[49] Therefore, the lower bound in the computation is $f_b - \sigma_{f_b}$. The upper bound is the Nyquist frequency because in the $\widetilde{CWT}$ computation we do not see any frequency component larger than 0.30.

Fig. 9 shows $P(t)$ for colloidal particles at some time t. One can see that particles surrounding the probe particle show relatively high power compared to particles far from the probe

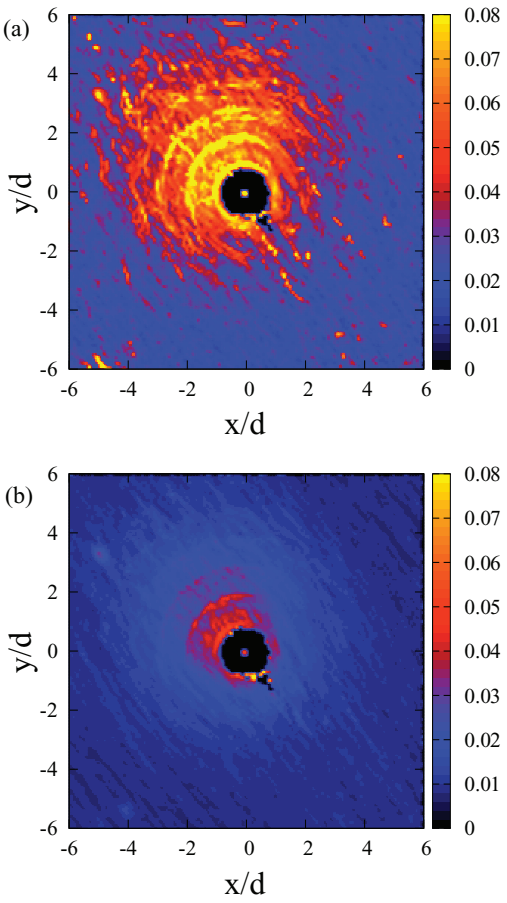

FIG. 10. (a) Spatial distribution of the maximum values in the power P encountered at each position over the domain $12d \times 12d$ with the probe particle located at the center. Particles having high power are mostly located in the forepart of the probe particle. (b) Spatial distribution of the averaged power P of particles shows that high powered particles commonly occurred up to the third neighboring shell in front of the center particle. For both computations, the cell size for spatial binning is chosen as $0.15d \times 0.15d$.

particle. From Video 2 in the supplementary material,[46] we also notice that some particles simultaneously exhibit high power for some time duration. In fact, near that duration the bond-orientational structures around those particles are distorted and these particles are coherently involved in cage breaking and formation dynamics through the response to the perturbation. Sometimes the particles in such a high power fluctuation form in a line, sometimes they are scattered, sometimes they are in a cluster including the probe particle.

In order to look into the spatial occurrence or organization of such transient high powered particles, we plot the spatial distribution of the maximum values in the power P encountered at each position over the entire snapshots in Fig. 10(a). The high powered particles are mostly located in front of the center particle with a forward radial pattern that expands to the remote region from the center particle. The pattern observed here is very similar to spatial fluctuation analysis of the same data in Ref. 26. Fig. 10(b) presents the spatial distribution of the averaged power P in which the average is taken over all the temporal P values of particles visiting in a space-fixed cell during the total observation time. This implies that even though some high powered particles appear in the regions remote from the probe particle they are relatively fewer and particles having high power mostly appear up to the third neighboring shell in front of the center particle. The results found in Fig. 10 shows the importance of the wavelet analysis, since such spatial pattern cannot be captured by the time averaged spatial correlation of $\bar{\psi}_6$ (Fig. 2 in the supplementary material[46]).

It may be obvious to have high powered particles in the first neighboring shell of the probe particle, since those particles always collide with the probe particle. However, it is

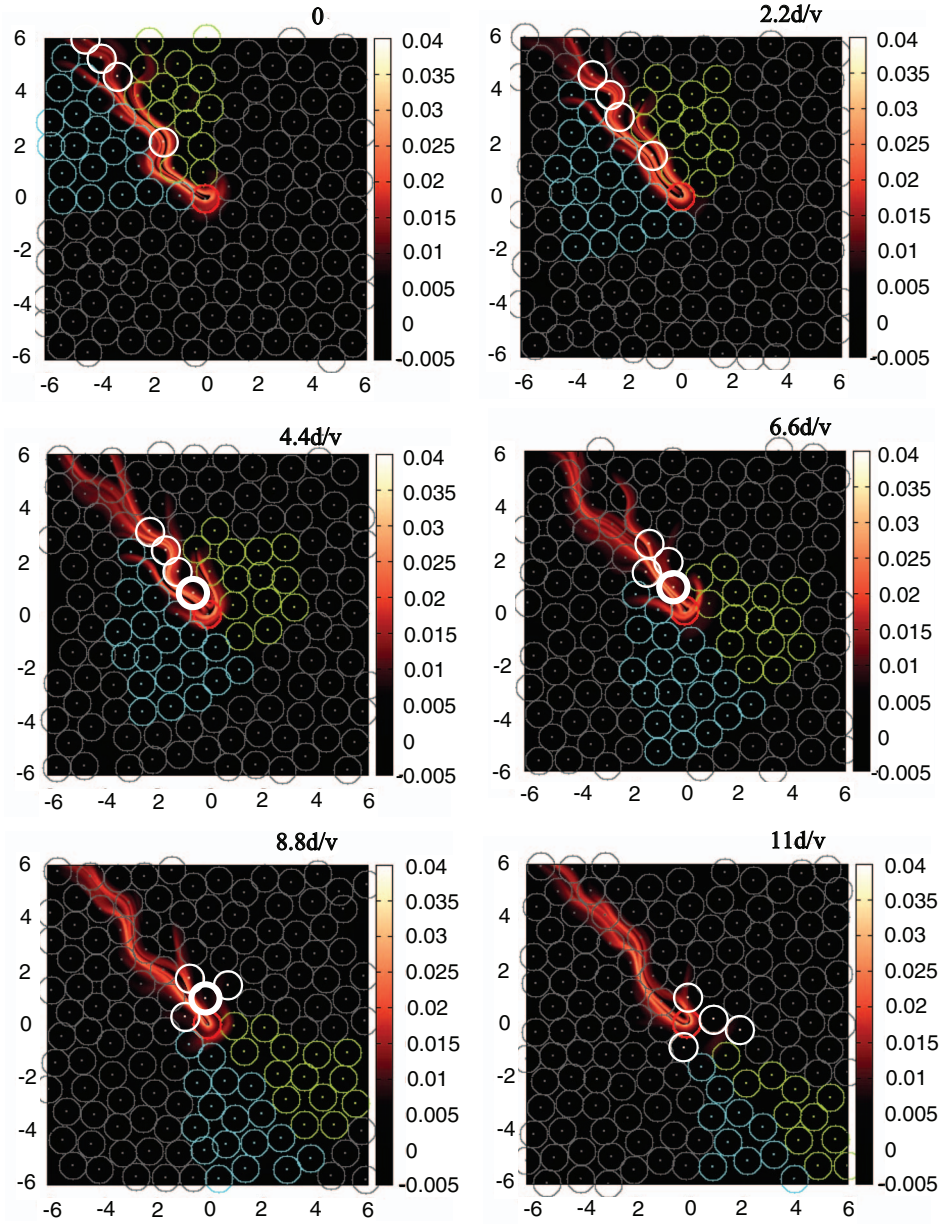

FIG. 11. Time evolution of the FTLE field with the superposition of colloidal particles. At the initial time $t = 0$, green, cyan, and white particles are identified corresponding to those in the right, and left of the FTLE/LCSs, and those sandwiched by the FTLE/LCSs, respectively. See Sec. III C 1.

far from trivial that high power regimes composed of particles far from the center particle are "changing from time to time," resulting in a cage breaking and formation dynamics.

C. FTLE/LCSs and dynamics of cage breaking and formation

In this section we analyze FTLE-based Lagrangian Coherent Structures to look into the dynamical foundation of the time dependent cage breaking and formation, and the question of why such spatial time-dependent organization of cage breaking and formation dynamics extends into the remote region.

1. FTLE/LCSs as separatrices

Here we consider the square domain ($12d \times 12d$) containing the probe particle at the center. For this square domain, the characteristic timescale of colloidal particles is $11d/v$. Note that choosing the integration time larger than this will make the FTLE ridges sharper and extend towards the dragging direction, i.e., top left direction. Fig. 11 demonstrates six consecutive snapshots of the FTLE field with the superposition of colloidal particles along the time propagation. First, one can see that the FTLE/LCSs, as forward FTLE ridges, exist in the forepart of the probe particle, which indicates that particles traveling and approaching to the probe particle experience some dynamical heterogeneity or frustration. In our investigation at some time instants, we have found that the most unstable directions turned out to be approximately normal to the FTLE/LCSs indicating repelling type LCSs (Fig. 1 in the supplementary material[46]). The most striking consequence of the application of the FTLE/LCSs is that they divide the colloidal flow into distinct regions of different dynamical characteristics. In this figure, we initially assigned a set of sample particles colored by cyan, green, and white corresponding to their positions relative to the FTLE/LCSs at time $t = 0$ (the origin of time is arbitrarily chosen) and look into their advection with the time evolution of the FTLE/LCSs. Cyan and green particles are identified according to the left and right of the FTLE/LCSs, respectively, and white particles are inside the foliation of the FTLE/LCSs. The gray particles are all the rest at $t = 0$ and also particles that flow into the domain. By monitoring the time evolution of the FTLE field with the superposition of the colloid (colored) particles, one can immediately see that by the time interval $11d/v$ white particles lag while green and blue particles move forward by leaving the white particles and the probe particle. This occurs because the motions of the white particles are retarded and get caught in the surrounding FTLE ridges for some time duration when they are traveling in front of the probe particle. In particular, one white particle, outlined by a bold white circle, in the vicinity of the probe particle becomes significantly stuck from $4.4d/v$ to $8.8d/v$ and gets lagged. This affects the motion of the other white particles coming behind.

2. FTLE/LCSs break particles arrangements in colloidal fluids

From the characteristics of the FTLE/LCSs, one can expect that the presence of the FTLE/LCSs in the vicinity of a particle causes a significant distortion of the cage near the corresponding particle. It is because particles on either side of the ridges will be separated from each other, resulting in the

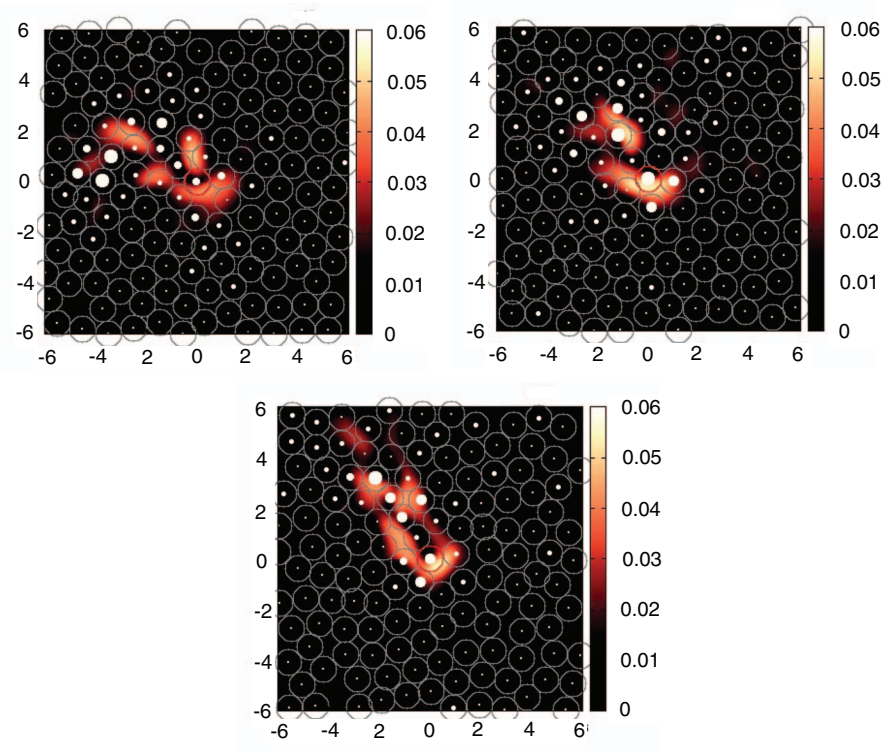

FIG. 12. Samples of the FTLE field ($T = d/v$) superimposed colloidal particles (gray circle). See Sec. III C 2.

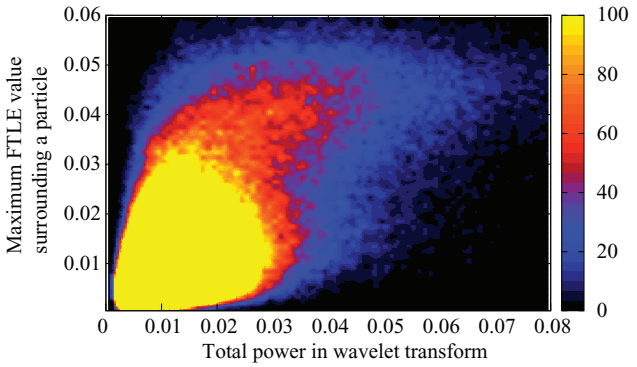

FIG. 13. 2D histogram with respect to the maximum values of FTLE field surrounding individual particles and powers of the particles in the wavelet transform. The color bar gives the number of points in each bin. Large population in the plot indicates the prevalent occurrence of no cage distortion at low FTLE field in the remote region. See Sec. III C 2.

breaking of ordered structures. Therefore, to establish a relationship between the FTLE/LCSs and the dynamics of cage breaking and formation discussed in Secs. III A and III B, we compute the FTLE field for the integration time corresponding to the timescale of the perturbation. This timescale is the same as that used in the wavelet analysis. Fig. 12 shows representative samples of the FTLE field with the superposition of colloidal particles indicated by gray circles. The size of the filled white circles inside the gray circles represents their power evaluated in the wavelet transform. Note that high-powered particles are more likely located near the FTLE ridges as expected, even when the particles are located far from the center particle (Video 3 in the supplementary material[46]).

This result indicates that if the FTLE/LCSs penetrate the surrounding structure of high powered particles, their surrounding structure will be broken during the integration timescale, i.e., the timescale of the perturbation. In order to establish this relationship between the FTLE/LCSs and cage breaking and formation evaluated by the power in wavelet transform, we investigate the correlation between the maximum values in the FTLE field surrounding the particles and powers of the particles. Fig. 13 presents a 2D histogram with respect to these two quantities. The correlation coefficient is found to be 0.667 with the standard error (s.e.) ±0.001, which

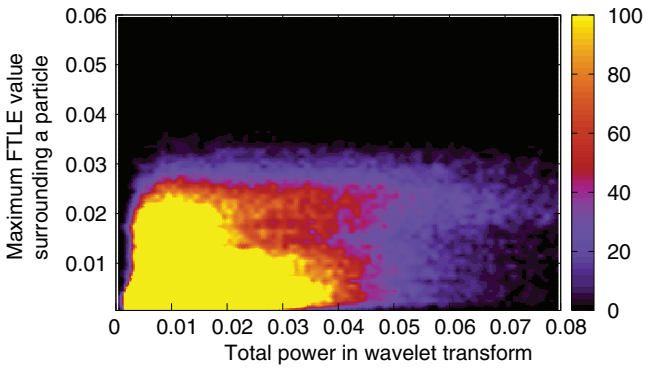

FIG. 14. 2D histogram for the same quantity as in Fig. 13 with 10 times longer integration time than the timescale of the perturbation. The correlation coefficient is $0.490 \pm 0.001 s.e.$

tells us that the concept of FTLE/LCSs plays a pivotal role for uncovering the mechanism of cage breaking and formation dynamics.

Fig. 14 also shows a 2D histogram for the same quantity as in Fig. 13, but in this case the integration time for the FTLE field is taken for 10 times longer than that in Fig. 13. It is found that, for this integration time, the correlation coefficient decreases to 0.49 compared to 0.667.

IV. CONCLUSION AND OUTLOOK

In this paper, we have presented a modified bond-orientational order parameter $\bar{\psi}_6$ which is free from discontinuities that cause difficulties with the standard ψ_6 parameter. This modified order parameter allows us to elucidate the spatio-temporal behavior of packing distortion associated with a particle's rearrangement. The key caution is that the value of the order parameter does not necessarily reflect the behavior of the particles in ordered/disordered region for the packing fraction of the system we studied. Rather, the time variation of the $\bar{\psi}_6$ parameter does. We found that particles that undergo packing distortion on the timescale of a perturbation contain high power in the wavelet analysis. The resulting cage breaking and formation dynamics can be considered a consequence of the system's mechanical response to the perturbation, which occurs in a highly anisotropic fashion (as seen in Fig. 10(a)). It should be noted that high-powered particles do not necessarily mean that they have been uncaged and are actively mobile at the same time, particularly in the remote region. Indeed, the presence of "dislocated" particle pairs[38] in this region trigger a cage breaking and formation surrounding a particle even though that particle does not move actively.

We have investigated the spatial occurrence of cage breaking dynamics in terms of FTLE-based LCSs. It was shown that FTLE/LCSs can probe the spatially heterogeneous dynamics in the colloidal system. In particular, particles whose motion is highly disturbed by the perturbation can be rationalized in terms of FTLE/LCSs. In this paper FTLE/LCSs were elucidated by the location of high amplitude in the FTLE field. However, the elucidation of characteristics of flows nearby the FTLE/LCSs is also crucial. One can intuitively think that in a system of constant dragging perturbation, the fluid parcel will be deformed in a way such that some particle will be stuck in front of the dragged particle and the nearby particles on either side will move passing through the stuck region, which may result in a sheared type deformation. However, our preliminary investigation, as exemplified in Fig. 1 in the supplementary material,[46] indicates that the most stretched directions of the deformation tensor are normal to the FTLE ridges, indicating repelling type LCSs. FTLE ridges that are extracted for backward time propagation provide approximations of attracting LCSs (in forward time propagation), to which nearby particles are attracted. Such attracting LCSs can also be of great importance in understanding the formation of a free volume and trailing wake behind the probe particle under the variation of dragging speed and/or Péclet number (the ratio of the shear rate of a flow to the particle's diffusion rate).

We expect that FTLE/LCSs may be a useful tool to quantify the dynamical correlation length in spatially heterogeneous dynamics near the jamming transition, and can probe the microscopic origin of the jamming transition. Since it is difficult to investigate directly the dynamics near the density regime where the jamming transition occurs, it is vital to develop a method to extrapolate results of our analysis in the lower density regime to those near the jamming transition. To extrapolate the results from lower density regime to a higher density regime, an appropriate choice of integration time may be important. For example, in a higher density regime, deformation timescales of fluid parcels are expected to be longer as the packing fraction increases. In a lower density regime, deformation timescales can be longer or shorter depending on the Péclet number. At lower packing fraction the hydrodynamic interaction dominates particle motions instead of direct collisions among particles. Therefore, the dynamics of the particles can be different depending on the hydrodynamic interaction and the system settings. In order to investigate them, a method to determine an appropriate integration time is needed.

Another possible application of FTLE/LCSs would be for understanding the dynamical behavior of particles and phase transition associated with rheological properties, such as shear thinning, Newtonian flow, and shear thickening of colloidal fluids. Application to shear thickening is expected to shed light on the lubrication hydrodynamics, formation of hydroclusters in the shear thickening regime,[50,51] and microviscosity in the field of active microrheology where the rheological properties are probed by single particle motion.[25]

ACKNOWLEDGMENTS

We thank Dr. Michio Otsuki for his valuable comments in our analysis of cage breaking and formation dynamics. This work has been supported by JSPS, Research Center for Computational Science, Okazaki, Japan, and Grant-in-Aid for challenging Exploratory Research (to T.K.), and Grant-in-Aid for Scientific Research (B) (to T.K.) from the Ministry of Education, Culture, Sports, Science and Technology. N.F.S. thanks the US National Science Foundation MRSEC (DMR082054) program for support.

[1] W. K. Kegel and A. van Blaaderen, Science **287**, 290 (2000).
[2] B. Cui, B. Lin, and S. A. Rice, J. Chem. Phys. **114**, 9142 (2001).
[3] O. Pouliquen, M. Belzons, and M. Nicolas, Phys. Rev. Lett. **91**, 014301 (2003).
[4] O. Dauchot, G. Marty, and G. Biroli, Phys. Rev. Lett. **95**, 265701 (2005).
[5] M. D. Ediger, Annu. Rev. Phys. Chem. **51**, 99 (2000).
[6] L. Berthier, Physics **4**, 42 (2011).
[7] C. A. Angell, Science **267**, 1924 (1995).
[8] G. Marty and O. Dauchot, Phys. Rev. Lett. **94**, 015701 (2005).
[9] C. Donati, J. F. Douglas, W. Kob, S. J. Plimpton, P. H. Poole, and S. C. Glotzer, Phys. Rev. Lett. **80**, 2338 (1998).
[10] C. Donati, S. C. Glotzer, P. H. Poole, W. Kob, and S. J. Plimpton, Phys. Rev. E **60**, 3107 (1999).
[11] N. Lačević, F. W. Starr, T. B. Schrøder, and S. C. Glotzer, J. Chem. Phys. **119**, 7372 (2003).
[12] A. R. Abate and D. J. Durian, Phys. Rev. E **76**, 021306 (2007).
[13] M. E. Cates, J. P. Wittmer, J.-P. Bouchaud, and P. Claudin, Phys. Rev. Lett. **81**, 1841 (1998).
[14] M. L. Falk and J. S. Langer, Phys. Rev. E **57**, 7192 (1998).
[15] A. R. Abate and D. J. Durian, Phys. Rev. E **74**, 031308 (2006).
[16] A. S. Keys, A. R. Abate, S. C. Glotzer, and D. J. Durian, Nat. Phys. **3**, 260 (2007).
[17] F. Lechenault, O. Dauchot, G. Biroli, and J. P. Bouchaud, EPL (Europhys. Lett.) **83**, 46003 (2008).
[18] K. A. Lorincz and P. Schall, Soft Matter **6**, 3044 (2010).
[19] R. Candelier and O. Dauchot, Phys. Rev. Lett. **103**, 128001 (2009).
[20] R. Candelier and O. Dauchot, Phys. Rev. E **81**, 011304 (2010).
[21] Y. Takehara, S. Fujimoto, and K. Okumura, EPL (Europhys. Lett.) **92**, 44003 (2010).
[22] P. Habdas and E. R. Weeks, Curr. Opin. Colloid Interface Sci. **7**, 196 (2002).
[23] P. Habdas, D. Schaar, A. C. Levitt, and E. R. Weeks, EPL (Europhys. Lett.) **67**, 477 (2004).
[24] L. G. Wilson, A. W. Harrison, A. B. Schofield, J. Arlt, and W. C. K. Poon, J. Phys. Chem. B **113**, 3806 (2009).
[25] I. Sriram, A. Meyer, and E. M. Furst, Phys. Fluids **22**, 062003 (2010).
[26] J. Pesic, J. Z. Terdik, X. Xu, Y. Tian, A. Lopez, S. A. Rice, A. R. Dinner, and N. F. Scherer, Phys. Rev. E **86**, 031403 (2012).
[27] E. Kolb, J. Cviklinski, J. Lanuza, P. Claudin, and E. Clément, Phys. Rev. E **69**, 031306 (2004).
[28] D. R. Nelson and B. I. Halperin, Phys. Rev. B **19**, 2457 (1979).
[29] D. R. Nelson and B. I. Halperin, Phys. Rev. B **21**, 5312 (1980).
[30] A. Jaster, Phys. Rev. E **59**, 2594 (1999).
[31] P. M. Reis, R. A. Ingale, and M. D. Shattuck, Phys. Rev. Lett. **96**, 258001 (2006).
[32] C. R. Berardi, K. Barros, J. F. Douglas, and W. Losert, Phys. Rev. E **81**, 041301 (2010).
[33] K. Watanabe and H. Tanaka, Phys. Rev. Lett. **100**, 158002 (2008).
[34] G. Haller and G. Yuan, Physica D **147**, 352 (2000).
[35] G. Haller, Physica D **149**, 248 (2001).
[36] S. C. Shadden, M. Astorino, and J.-F. Gerbeau, Chaos **20**, 017512 (2010).
[37] S. Raben, S. Ross, and P. Vlachos, Exp. Fluids **55**, 1638 (2013).
[38] J. S. Olafsen and J. S. Urbach, Phys. Rev. Lett. **95**, 098002 (2005).
[39] B. Aldridge, G. Haller, P. Sorger, and D. Lauffenburger, IEE Proc.: Syst. Biol. **153**, 425 (2006).
[40] M. Astorino, J. Hamers, S. C. Shadden, and J.-F. Gerbeau, Int. J. Numer. Meth. Biomed. Eng. **28**, 937 (2012).
[41] J. Peng and J. O. Dabiri, J. Fluid Mech. **623**, 75 (2009).
[42] T. Peacock and J. Dabiri, Chaos **20**, 017501 (2010).
[43] S. C. Shadden, F. Lekien, and J. E. Marsden, Physica D **212**, 271 (2005).
[44] G. Haller and T. Sapsis, Chaos **21**, 023115 (2011).
[45] Recently, G. Haller [Physica D **240**, 574 (2011)] has defined LCSs rigorously in terms of hyperbolic material surfaces with extreme finite time repulsion and extraction, to avoid spurious identification of LCSs that appear due to shear or stretching.
[46] See supplementary material at http://dx.doi.org/10.1063/1.4894866 for the time evolution of $\bar{\psi}_6$ (Video 1), the power of particles (Video 2), and the FTLE field with the superposition of the power of particles (Video 3). All movies are created for a few hundred frames. In addition, Figs. 1 and 2 are shown for the maximal stretching directions along the FTLE ridges, and the time averaged spatial correlation of $\bar{\psi}_6(t)$, respectively.
[47] P. S. Addison, *The Illustrated Wavelet Transform Handbook* (Institute of Physics Publishing, 2002).
[48] D. Gabor, J. Inst. Electr. Eng. - Part III: Radio Commun. Eng. **93**, 429 (1946).
[49] The Fourier transform of the Gabor wavelet is given by $\Phi(f) = \frac{\nu}{f_b} \exp[-\pi(\frac{\nu(f-f_b)}{f_b})^2]$ that is a Gaussian form of frequency f with mean f_b and the standard deviation $\sigma_{f_b} = \frac{1}{\sqrt{2\pi}} \frac{f_b}{\nu}$. Here σ_{f_b} provides the amount uncertainty to the identification of f_b in the frequency plane. As ν is smaller (larger), the uncertainty becomes larger (smaller) in frequency (while the uncertainty in time (scale) becomes smaller (larger) in the wavelet transform). In our analysis, the time scale of perturbation is about 14 frames. In our study, we set two conditions to decide the value of ν: to have time resolution at least 14 frames which can be captured by choosing $\nu \leq 1$, and to distinguish the base frequency f_b to the other frequency components. In this sense, The value of ν less than 1 will increase the uncertainty in frequency which makes it difficult to differentiate the b.
[50] J. R. Melrose and R. C. Ball, J. Rheol. **48**, 961 (2004).
[51] X. Cheng, J. H. McCoy, J. N. Israelachvili, and I. Cohen, Science **333**, 1276 (2011).